



# Modeling of second-order spectrophotometric data generated by a pH-gradient flow injection technique for the determination of doxorubicin in human plasma



Mirta R. Alcaráz, Agustina V. Schenone, María J. Culzoni, Héctor C. Goicoechea \*

Laboratorio de Desarrollo Analítico y Quimiometría (LADAQ), Cátedra de Química Analítica I, Facultad de Bioquímica y Ciencias Biológicas, Universidad Nacional del Litoral-CONICET, Ciudad Universitaria, 3000 Santa Fe, Argentina

## ARTICLE INFO

### Article history:

Received 8 August 2013

Received in revised form 16 September 2013

Accepted 17 September 2013

Available online 25 September 2013

### Keywords:

Multivariate curve resolution

Doxorubicin

Human plasma

Second-order calibration

## ABSTRACT

In this paper, the development of a pH-gradient flow-injection method with diode-array spectrophotometric detection combined with extended multivariate curve resolution-alternating least-squares (MCR-ALS) to quantitate doxorubicin in the presence of rifampicin in plasma samples is presented.

Quantitation of doxorubicin was based on acid–base and spectral differences between its species and those for the interference. Overlapped profiles among the analyte and the interference were mathematically solved by data modeling with the well-known extended MCR-ALS algorithm.

The method, which involves a simple sample pretreatment consisting in the addition of trichloroacetic acid followed by centrifugation, was applied to resolve validation mixtures composed of human plasma spiked with doxorubicin. Acceptable analytical figures of merit were obtained, i.e. recoveries from 96 to 107%, coefficients of variation between 0.2% and 7.8%, and limits of detection and quantification of 0.77 and 2.32  $\mu\text{g L}^{-1}$ , respectively.

© 2013 Elsevier B.V. All rights reserved.

## 1. Introduction

Doxorubicin (DXR) is an anthracycline antibiotic produced by *Streptomyces peucetius varietal caesioides*. Due to its broad spectrum antineoplastic activity, DXR is one of the most important anticancer agents currently in use [1–4]. From a medical or clinical point of view, monitoring drug levels in body fluids such as urine and plasma has become increasingly demanded in order to assess toxicity, adverse effects, interactions and therapeutic efficiency.

A variety of HPLC procedures to resolve and quantitate DXR and its metabolites in pharmaceutical dosage forms and biological fluids have been published [5–11]. Several approaches for the quantitation of DXR and other anticancer agents in biological fluids, including capillary electrophoresis, UV–visible spectroscopy and HPLC techniques, have been summarized by Zagotto et al. [12]. Recently, a rapid analysis of DXR and daunorubicin using microchip capillary electrophoresis was developed by Lu and co-workers [13]. In spite of providing satisfactory results, many of these techniques are laborious and time consuming. On the other hand, flow-injection analysis (FIA) and other related flow techniques with diode-array spectrophotometric detection can be used to generate large amounts of data of different dimensions, i.e. data ranging from traditional peak-height values to multivariate vectors and matrices that comprise instrumental responses in the temporal and/or

spectral domains, in a very simple and fast way [14,15]. However, due to the fact that FI methods do not physically separate components that flow together and reach the detector concurrently, their combination with alternative techniques is necessary to ensure selectivity. Numerous methods regarding the coupling of FIA systems to chemometric modeling aimed at determining one or several analytes in a rapid, simple and inexpensive way have been published [16–19]. Furthermore, the capabilities of FIA in combination with chemometric methods to simultaneously determine several analytes present in multicomponent drugs were discussed by Saurina [20]. Analyte quantitation in the presence of responsive interferences can be performed by measuring second-order signals and processing them with appropriate multivariate algorithms to achieve the second-order advantage [21]. Direct determination of DXR in human plasma based on fluorescence recording of excitation–emission matrices coupled to the multiway chemometric methods PARAFAC and N-PLS was accomplished [22]. Very recently, quantitation of DXR in human plasma has been performed by using total synchronous fluorescence spectroscopic data modeled with the first- and second-order algorithms [23].

In this paper, a pH-gradient FI method with diode-array spectrophotometric detection for the determination of DXR in plasma samples in the presence of rifampicin (RFP) is presented. RFP is a semisynthetic compound derived from *Amycolatopsis rifamycinica* typically used to treat *Mycobacterium* infections, including tuberculosis and Hansen's disease. Considering that the spectrum of RFP highly overlaps with those of DXR, RFP was selected as the uncalibrated interference with the aim of

\* Corresponding author. Tel.: +543424575205.

E-mail address: [hgoico@fcb.unl.edu.ar](mailto:hgoico@fcb.unl.edu.ar) (H.C. Goicoechea).

evaluating the potentiality of the method to accurately quantitate the analyte in extreme conditions. The instrumental responses recorded over two measurement domains, i.e. spectral and temporal, were arranged in data matrices and subjected to the extended multivariate curve resolution method based on alternating least squares (MCR-ALS).

Deprotonation constants ( $K_a$ ) of ionizable compounds are important properties that describe the charge state of the drug at a certain pH. This information is essential in the estimation of the pharmacokinetic and pharmacodynamic properties of drugs, since they may considerably vary according to the different protonation/ionization forms of the molecules. Moreover,  $K_a$  values of ionizable drugs affect their lipophilicity and permeability, which are important physical and chemical features to be considered in order to predict bioavailability [24]. For this reason, the determination of the  $pK_a$  values of DXR was also accomplished in the present work by the application of an UV-Vis spectrophotometric titration technique.

## 2. Experimental

### 2.1. Apparatus

The FIA system was developed using five modules (degasser, pump, injection valve, autosampler and DAD detector) of an Agilent 1100 Series instrument (Agilent Technologies, Waldbronn, Germany). The carrier buffer (CB) was pumped through an 800 mm length and 0.5 mm i.d. flexible mixing coil flowing at  $0.5 \text{ mL min}^{-1}$ . Spectra were registered in the range of 300–800 nm each 2 nm. In this way, absorbance–time matrices were of size  $174 \times 251$ . These matrices were saved in ASCII format, and transferred to a PC based on an Intel® Core™ i7 microprocessor for subsequent manipulation.

The pH of solutions was measured with an Orion (Massachusetts, United States) 410 A potentiometer equipped with a Boeco (Hamburg, Germany) BA 17 combined glass electrode.

Absorbance measurements were obtained with a PerkinElmer (Waltham, Massachusetts, USA) Lambda 20 spectrophotometer.

### 2.2. Software

Multivariate methods discussed in the present work were run in MATLAB 7.9 [25]. MCR-ALS algorithms were implemented using the graphical interface downloaded from [www.mcrals.info](http://www.mcrals.info). Deprotonation constants were determined using the PKFIT program [26], which is based on a full-spectrum least-squares procedure, and can be obtained from the authors on request.

### 2.3. Reagents and solutions

Doxorubicin hydrochloride (94.0%) was obtained from Richmond Laboratory S.A.C.I.F. (Pilar, Buenos Aires, Argentina). Rifampicin (99.4%) was obtained from Laboratory of Pharmaceutical Quality Control (Faculty of Biochemistry and Biological Sciences, National University of Litoral, Argentina). Sodium phosphate monobasic, sodium hydroxide, hydrochloric acid, phosphoric acid and sodium carbonate were purchased from Cicarelli (San Lorenzo, Santa Fe, Argentina). Trichloroacetic acid (TCA) was obtained from Anedra (San Fernando, Argentina). Ultrapure water was obtained from a Milli-Q water purification system from Millipore (Bedford, MA, USA).

A  $70 \text{ } \mu\text{g mL}^{-1}$  stock solution was prepared by dissolving the appropriate amount of DXR in ultrapure water. This solution was stored in a glass bottle at  $4 \text{ }^\circ\text{C}$ , protected from light, for a maximum period of 3 days. A  $620 \text{ } \mu\text{g mL}^{-1}$  stock solution of RFP was prepared by dissolving the suitable amount of drug in 1% phosphoric acid, and stored at  $4 \text{ }^\circ\text{C}$ .

The  $0.5 \text{ mol L}^{-1}$  CB solution was prepared by dissolving the suitable amount of  $\text{Na}_2\text{CO}_3$ , adjusting the pH to 9.5 with  $1 \text{ mol L}^{-1}$  HCl, and diluting to the mark with ultrapure water in a 500.0 mL volumetric

flask. The  $0.5 \text{ mol L}^{-1}$  sample buffer (SB) was prepared by dissolving the appropriate quantity of  $\text{Na}_2\text{CO}_3$ , adjusting the pH to 6.0 with  $1 \text{ mol L}^{-1}$  HCl, and diluting to the mark with ultrapure water in a 50.0 mL volumetric flask.

Heparinized human plasma samples from untreated healthy volunteers were obtained from Hospital Iturraspe of Santa Fe City, Argentina, and stored at  $-20 \text{ }^\circ\text{C}$  until the experiments were performed.

### 2.4. Spectrophotometric titration

The spectrophotometric titration was conducted on an acidified solution (pH  $\sim 4$ ) containing  $23.0 \text{ } \mu\text{g mL}^{-1}$  of DXR. The general procedure involved the addition of small aliquots of  $0.01$  or  $5 \text{ mol L}^{-1}$  NaOH to 50.0 mL of the stirred original solution, in order to obtain small pH increments. As each new pH point was reached, the corresponding spectrum was acquired by extracting 2 mL of solution from the vessel, which were then restored, until pH  $\sim 13$  was achieved. At the end of the titration, approximately 40 spectra were recorded, which were subsequently processed by means of the PKFIT program.

### 2.5. Calibration and validation samples

A calibration set composed of five standard samples was prepared in triplicate by transferring appropriate aliquots of DXR stock solution to 2.0 mL volumetric flasks and completing to the mark with heparinized human plasma. After vortex mixing, solutions were allowed standing for 30 min to reach equilibrium. Then, plasma deproteinization was performed by adding  $200 \text{ } \mu\text{L}$  of 50% TCA acid to each calibration solution and centrifuging for 20 min at 3000 rpm. Subsequently,  $600 \text{ } \mu\text{L}$  aliquots of each solution and  $200 \text{ } \mu\text{L}$  of SB were transferred to Eppendorf® tubes. The mixtures were centrifuged for 5 min at 10,000 rpm. After completing the latter experimental procedure, the final concentrations of the calibration samples were between 1.5 and  $15.0 \text{ } \mu\text{g mL}^{-1}$ . Eventually,  $500 \text{ } \mu\text{L}$  aliquots of each sample were transferred to vials, and  $100 \text{ } \mu\text{L}$  were injected into the FIA system.

A 6-sample validation set was built considering concentrations of DXR different than those used for calibration, and following a random design. Besides, the interference RFP was incorporated at different concentrations in samples 3 to 6 ( $10.7$ ,  $14.3$ ,  $12.5$  and  $10.0 \text{ } \mu\text{g mL}^{-1}$ , respectively).

A 27-sample precision set was prepared at three different concentration levels ( $4.0$ ,  $7.0$  and  $12.0 \text{ } \mu\text{g mL}^{-1}$ ) in triplicate, and in three different weeks.

The validation and precision sets were prepared by transferring appropriate aliquots of stock solution of DXR for precision samples, and DXR and RFP for validation samples to 2.0 mL volumetric flasks and completing to the mark with plasma. Then, these solutions were processed in the same way as the calibration samples.

## 3. Theory

### 3.1. MCR-ALS

One of the most interesting properties of this algorithm is its capability of dealing with data sets deviating from trilinearity. Instead of forming a three-dimensional data array, the latter is unfolded along the mode that is suspected of breaking the trilinear structure, i.e. if a matrix-to-matrix variation of profiles occurs along the column direction, a column-wise augmented matrix is created. The bilinear decomposition of the augmented matrix **D** is performed according to the expression:

$$\mathbf{D} = \mathbf{C} \times \mathbf{S}^T + \mathbf{E} \quad (1)$$

where the rows of **D** contain the absorption spectra measured as a function of time, the columns of **C** contain the time profiles of the

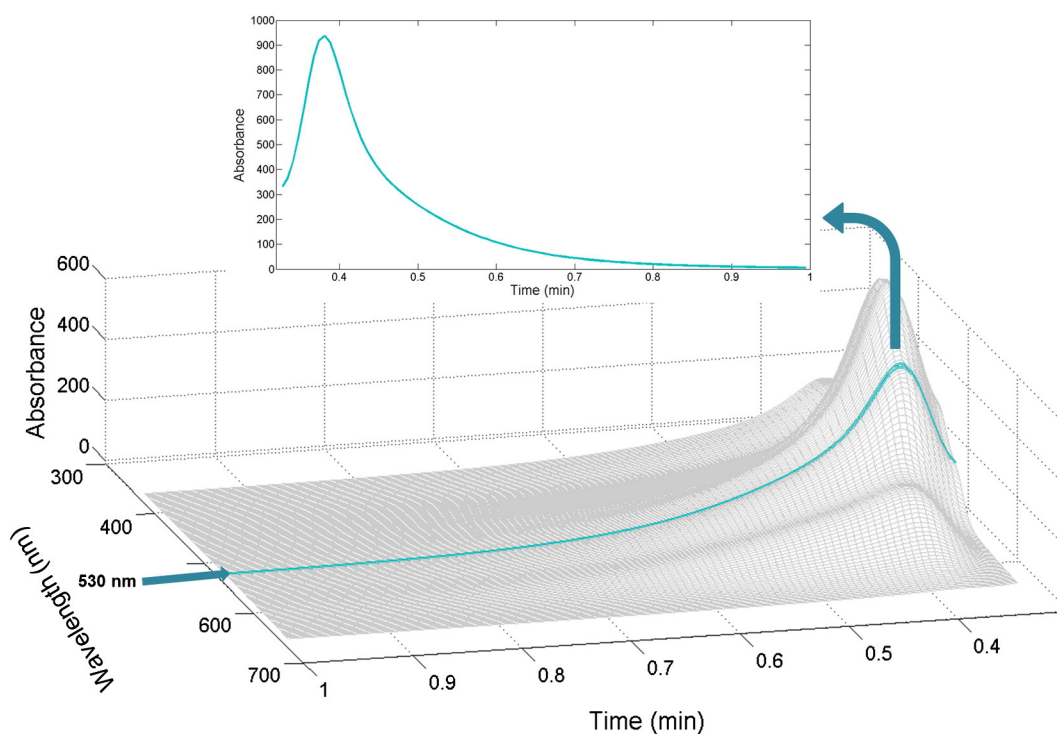


Fig. 1. Representation of how the closure vector is obtained for a calibration sample data matrix.

compounds involved in the process, the columns of **S** their related spectra, and **E** is a matrix of residuals not fitted by the model. Appropriate dimensions of **D**, **C**, **S**, and **E** are thus  $(1 + I) K \times J$ ,  $(1 + I) KJ \times K$  and  $(1 + I) K \times J$ , respectively ( $I$  = number of calibration samples).

Decomposition of **D** is achieved by iterative least-squares minimization of  $\|E\|$  under suitable constraining conditions (non-negativity in spectral profiles, unimodality and non-negativity in concentration profiles, and closure).

Typically **D** is built by placing one on top of another calibration submatrices and each of the test submatrices. While the pure spectrum of each compound should be the same in all experiments and the spectral mode must be selective, the temporal profiles in the different **C** submatrices need not to share a common shape.

In the present context, it is necessary to point out that MCR-ALS requires initialization with system parameters as close as possible to the final results. The spectra of the species are required in the column-wise augmentation mode, as obtained from either pure analyte standards or from the analysis of the purest spectra based on the so-called SIMPLISMA (simple interactive self-modeling mixture analysis) methodology [18], which is an MCR algorithm useful to extract pure component spectra from a series of spectra of mixtures of varying composition.

Finally, successful MCR is also aided by the inclusion of information about the correspondence among species in each matrix (i.e. information as to whether a given component exists or not in a given sample).

### 3.2. Calculation of pH gradient in FIA

A temporal region from 20 to 60 s (0.33 to 1 min) was selected for the calculation of the pH gradient, in which both acidic and basic species were simultaneously detected in the system. Several single calibration matrices were used in order to obtain the gradient.

Three constraints were applied during the ALS optimization of the species profiles in matrices **C** and **S<sup>T</sup>**. These constraints were non-negativity in spectral and concentration profiles, and variable closure in concentration profiles. The second constraint is further explained in more detail.

For an accurate calculation of pH values, the concentration of the acidic and basic species (referred to as [HD] and [D], respectively) in the FI peak should be recovered without scale or intensity ambiguities. In acid–basic equilibrium, the whole system should fulfill mass-balance and mass-action laws. For a particular compound, its analytical concentration  $C_D$  is the sum of the concentration of the acidic HD and basic species D;  $C_D = [HD] + [D]$ . In the flow-injection system under study, the sample injection into the carrier stream produced a dispersion of the analyte along the peak with a non-constant total  $C_D$  over time. However, at each point of the process the mass-balance equation between species was still obeyed. A good estimation of the  $C_D$  shape variation in the FI peak was obtained from the absorbance variation of one standard sample at an isobestic wavelength. The latter was chosen because in the isobestic wavelength both species have the same absorbance, so at each point of the process, the sum of their concentrations should be equal to the total analyte concentration estimated from the isobestic point. This estimate was used as a closure vector during the ALS optimization. Fig. 1 shows how the selected closure vector was obtained at 530 nm from the experimental data matrix. The proper use of all of these constraints drastically reduces the rotational and intensity

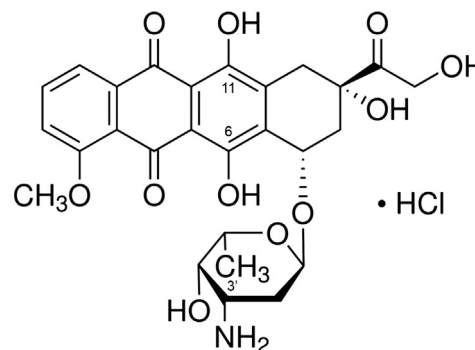
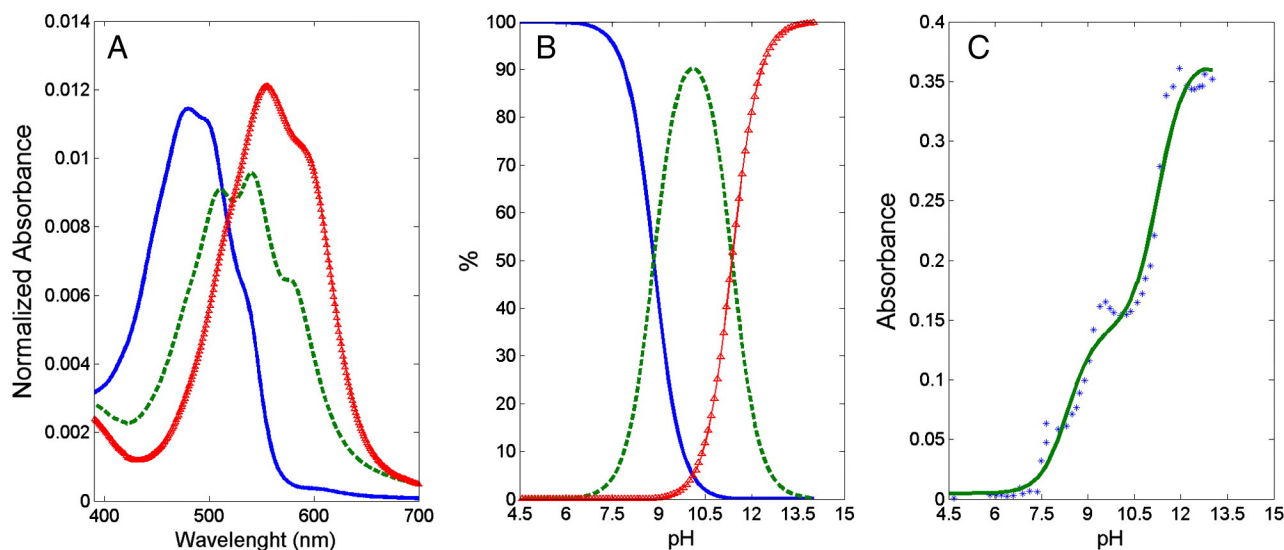


Fig. 2. Chemical structure of DXR.



**Fig. 3.** PKFIT results. (A) Spectra of the three species of DXR (solid blue line: acidic form; dashed green line: amphiphilic form; and dotted red line: basic form). (B) Distribution of species for DXR (solid blue line: acidic form; dashed green line: amphiphilic form; and triangles red line: basic form). (C) Titration curve (blue triangles: experimental result at 400 nm; solid green line: fitted curve). (For interpretation of the references to color in this figure legend, the reader is referred to the web version of this article.)

ambiguities associated with the decomposition of the experimental data matrix [28].

In order to establish the relationship between measured times and pH values, a standard solution of DXR with  $pK_{a1}$  value previously obtained with the PKFIT program was used. Once the concentration profile was retrieved by MCR-ALS, the concentration of each species was obtained at each time, and the pH profile was obtained as follows:

$$\text{pH} = pK_{a1} - \log \frac{[\text{HD}]}{[\text{D}]} \quad (2)$$

in which  $pK_{a1}$  is the first acidity constant of DXR.

An advantage of this procedure is that there is no need of performing experimental pH measurements.

## 4. Results and discussion

### 4.1. Spectral characteristics of DXR

Previous to the quantitative study, and in order to establish adequate working conditions, both the absorption features of DXR and its acid-base behavior were evaluated.

DXR has three significant prototropic functions with associated  $pK_a$ s: (1) the amino group in the sugar moiety ( $pK_{a1} = 8.15$ ), (2) the phenolic group at C11 ( $pK_{a2} = 10.16$ ), and (3) the phenolic group at C6 ( $pK_{a3} = 13.2$ ) [29]. At  $\text{pH} < 8$  DXR presents a characteristic orange color with a maximum at 475 nm. On the other hand, at  $\text{pH} > 9$  the absorbance maximum is located at around 550 nm, which is related to its violet color. Fig. 2 displays the chemical structure of DXR.

The deprotonation constants of DXR in the ground state could be determined from pH titration multi-wavelength spectrophotometric data. Fig. 3 shows the variation of the absorbance vs. pH, the distribution of species and the titration curve obtained by means of the PKFIT program. As can be seen in Fig. 3A, three species are present in the system, i.e. acidic, amphiphilic and basic species. The distribution of these species appreciated in Fig. 3B reveals the existence of two deprotonation constants ( $pK_{a1} = 8.84$  and  $pK_{a2} = 11.36$ ). In Fig. 3C, the same conclusion can be reached by inspection of the inflection points situated in those pH values.

### 4.2. Flow-injection system

In this work, the sample dispersion was responsible for the generation of a double pH gradient after the sample merged with the basic carrier. It can be appreciated in Fig. 4 how the pH decreases from the front of the flow-injection peak reaching its minimum value at the center of the sample bolus, and then progressively increases to reach its original pH value.

### 4.3. Calculation of pH gradient

Due to the fact that the instrument used to perform FIA does not allow working at  $\text{pH} > 10$ , the pH range was restricted from 6.0 to 9.5. Therefore, only the acidic and amphiphilic species were observed within this pH range given by the value of DXR  $pK_{a1}$  (8.84). Because the basic form is not present in this pH range, from this point forward, the amphiphilic species will be considered as the basic species for labeling purposes.

In order to study the behavior of DXR and the pH gradient profile generated in the flow-injection system, all the matrices used for this purpose were restricted in the time direction from 20 to 60 s (0.33 to 1 min), where both acidic and basic species were simultaneously present in the system, and in the spectral dimension from 370 to 650 nm. Five single matrices corresponding to the five calibration samples (one replicate was used for each concentration level) were analyzed separately with MCR-ALS in order to obtain this gradient.

When applying singular value decomposition (SVD) to determine the correct number of compounds in the model, it was not possible to detect the right number of contributing components which explain the variance of the system, because in this case, the number retrieved

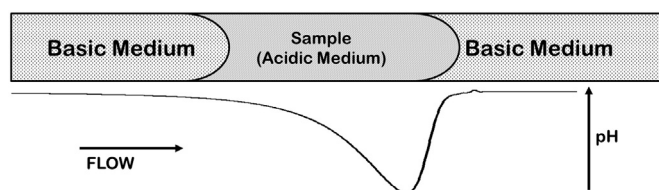


**Fig. 4.** Scheme of the pH gradient profile.

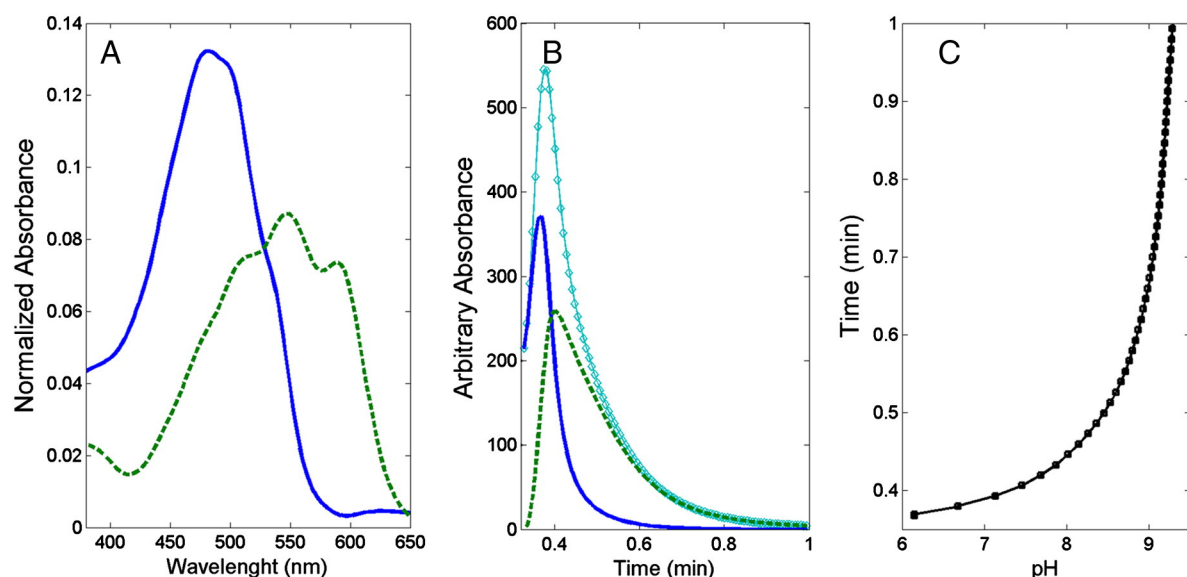


**Fig. 5.** (A) MCR-ALS spectral profiles (solid blue line: acidic form; dashed green line: basic form). (B) MCR-ALS FIA profiles (solid blue line: acidic form; dashed green line: basic form) and closure vector (diamond cyan line). (C) Resolved pH gradient profile. (For interpretation of the references to color in this figure legend, the reader is referred to the web version of this article.)

by SVD was higher than the real one due to spectral combination of the acidic and basic species. The plasma does not present absorbance in the wavelength region under study. Therefore, two components were used. To build the initial estimations, the spectra of the acidic and basic species were obtained from the analysis of the purest spectra based on the SIMPLISMA methodology [27].

The flow-injection peak profile of DXR at 530 nm, which was restricted to the same temporal region of the data matrix, was used as

the total concentration profile, i.e. as a closure vector. Non-negativity in concentration and spectral profiles was also applied to constrain the ALS procedure. The spectra of both species recovered in these conditions are shown in Fig. 5A. The obtained concentration profile and the closure vector can be observed in Fig. 5B, being the latter the sum of the contribution of both species. As explained in Section 3.2, the gradient profile depends on time, and this trend can be observed in Fig. 5C.

With the aim of analyzing the pH gradient profile of five different data matrices, the time in which the concentration of both species remained the same ( $\text{pH} = \text{pK}_{a1}$ ) was taken into account. Therefore, the latter was accomplished at  $23.5 \pm 0.1$  s ( $\pm$  term refers to the confidence interval for  $n = 5$  experimental points, 4 degrees of freedom, at a significance level  $\alpha = 0.05$ ).

**Table 1**  
Analytical figures of merit.

Figures of merit	MCR-ALS
Lineal range ( $\mu\text{g mL}^{-1}$ )	1.5–12.0
Intercept $\pm$ SD <sup>a</sup>	$(-28 \pm 4) \times 10^3$
Slope $\pm$ SD <sup>a</sup> ( $\text{L } \mu\text{g}^{-1}$ )	$30 \pm 1$
Determination coefficient ( $r^2$ )	0.994
$\gamma^b$ ( $\text{L } \mu\text{g}^{-1}$ )	2.6
Inverse of analytical sensitivity ( $\gamma$ ) <sup>-1</sup> ( $\mu\text{g L}^{-1}$ )	0.23
LOD <sup>c</sup> ( $\mu\text{g L}^{-1}$ )	0.77
LOQ <sup>d</sup> ( $\mu\text{g L}^{-1}$ )	2.32

<sup>a</sup> SD: Standard deviation for  $n - 1$  degree of freedom.

<sup>b</sup> Analytical sensitivity.

<sup>c</sup> LOD: Limit of detection calculated according to Ref [30].

<sup>d</sup> LOQ: Limit of quantification calculated as  $\text{LOD} \times (10/3.3)$ .

#### 4.4. Calibration and validation: analytical figures of merit and predictions

##### 4.4.1. Sensitivity, limit of detection and limit of quantitation

For both calibration and validation studies, the data generated in each sample injection were restricted in the same way as in the previous section, i.e. 20 to 60 s (0.33 to 1 min) in time direction and 370 to 650 nm in wavelength direction.

In order to quantitate the analyte concentration, a **D** augmented matrix was built by appending the second order calibration data matrices. During the ALS optimization the following constraints were applied to

**Table 2**  
Results obtained when analyzing the precision set, coefficients of variation and ANOVA probabilities.

DXR ( $\mu\text{g mL}^{-1}$ )	Week 1			Week 2			Week 3			ANOVA <sup>b</sup> ( $p$ -value)
	Prediction	Average	CV% <sup>a</sup>	Prediction	Average	CV% <sup>a</sup>	Prediction	Average	CV% <sup>a</sup>	
4.0	4.2	4.0	5.2	4.3	4.3	1.4	4.4	4.3	3.6	0.178
	4.1			4.2			4.3			
	3.8			4.3			4.1			
7.0	8.3	8.0	4.5	8.4	8.4	0.2	8.4	8.5	0.7	0.079
	8.1			8.4			8.5			
	7.6			8.4			8.5			
12.0	13.4	12.4	7.8	12.3	13.1	5.6	13.8	14.0	1.5	0.085
	12.2			13.7			14.2			
	11.5			13.4			13.9			

<sup>a</sup> CV%: Percentage variation coefficient.  $\text{CV}\% = (\text{SD}/\text{average conc.}) \times 100$ , in which SD is the standard deviation for  $n - 1$  degree of freedom.

<sup>b</sup> Analysis of variance: all the means are equal when  $p > 0.05$ .

**Table 3**  
Determination of DXR in the validation samples.

DXR						RFP
Sample	Nominal ( $\mu\text{g mL}^{-1}$ )	Predicted FIA ( $\mu\text{g mL}^{-1}$ ) $\pm$ SD <sup>a</sup>	Predicted HPLC ( $\mu\text{g mL}^{-1}$ ) $\pm$ SD <sup>a</sup>	Mean recovery (%) FIA/HPLC	$t_{(3,0.05)}$ (p) <sup>b</sup>	Nominal ( $\mu\text{g mL}^{-1}$ )
1	6.0	6.4 $\pm$ 0.3	–	106	–	–
2	10.0	9.6 $\pm$ 0.7	–	96	–	–
3	8.0	7.9 $\pm$ 0.1	–	99	–	10.7
4	7.5	7.7 $\pm$ 0.1	7.5 $\pm$ 0.1	109/100	2.47 (0.09)	14.3
5	6.0	6.3 $\pm$ 0.1	6.08 $\pm$ 0.04	105/101	2.84 (0.07)	12.5
6	5.5	5.6 $\pm$ 0.1	–	102	–	10.0
RMSE <sup>c</sup> ( $\mu\text{g mL}^{-1}$ )			0.22			
REP <sup>d</sup>			3.1			
$t_{\text{calculated}}$ <sup>e</sup>			–0.697 (0.517)			

<sup>a</sup> SD: Standard deviation.

<sup>b</sup>  $t$  value obtained for means comparison ( $\nu = 3 - 1$  and  $\alpha = 0.05$ ). Between parenthesis is the probability value.

<sup>c</sup> RMSE: Root mean square error,  $\text{RMSE} = \left[ \frac{1}{I} \sum_{i=1}^I (c_{\text{act}} - c_{\text{pred}})^2 \right]^{1/2}$ , where  $I = 6$ .

<sup>d</sup> REP: Relative error of prediction,  $\text{REP} = 100 \times \text{RMSE} / \bar{c}$ , where  $\bar{c}$  is the mean calibration concentration.

<sup>e</sup>  $t$  value obtained from paired  $t$ -test with  $\alpha > 0.05$ . Between parenthesis is the probability value.

get physically meaningful solutions: (a) the concentration and spectra profiles were non-negative, and (b) correspondence between common species in the different data matrices. In this FI system, the unimodality constraint in the concentration profile is not applicable. After MCR–ALS decomposition of **D**, the concentration information contained in **C** was used to construct the pseudounivariate graph by plotting the analyte concentration scores against the nominal analyte concentrations. The analyte concentration score can be defined as the area under the profile for the  $i$ th sample:

$$a(i, n) = \sum_{j=1+(i-1)J}^{iJ} \mathbf{C}(j, n) \quad (3)$$

in which  $a(i, n)$  is the score for the component  $n$  in the sample  $i$ . In this work, the acidic specie was used for all the following studies, because it has higher sensitivity in the whole concentration range.

Sensitivity (SEN), defined as the variation in net response for a given change in analyte concentration, can be considered as one of the most relevant figures of merit in the field of analytical chemistry due to the fact that it is a decisive factor in estimating others, such as limit of detection (LOD) and limit of quantitation (LOQ).

According to Bauza and coworkers [30], the following expression estimates the SEN when extended MCR–ALS is applied:

$$\text{SEN}_{\text{MCR}} = m_n \left[ J(\mathbf{S}^T \mathbf{S})_{nn}^{-1} \right]^{-1/2} \quad (4)$$

in which  $n$  is the index for the analyte of interest in a multicomponent mixture,  $m_n$  is the slope of the MCR pseudounivariate calibration graph for this analyte,  $\mathbf{S}^T$  is a matrix containing the profiles for all sample components in the non-augmented MCR direction, and  $J$  is the number of channels in the test sample data matrix in the augmented MCR direction. Table 1 summarizes the obtained figures of merit.

DXR is usually injected as a dose of 60–75 mg  $\text{m}^{-2}$ , giving an initial concentration of about 20  $\mu\text{g mL}^{-1}$  in an adult male. Only a fraction of this injected drug will be present in the plasma [22]. As can be observed, the LOQ value (2.32  $\mu\text{g L}^{-1}$ ) is below the plasmatic DXR concentration usually found in treated patients with cancer.

#### 4.4.2. Precision study: repeatability and intermediate precision

Table 2 summarizes the results of the precision study carried out on the precision test samples. For this purpose, repeatability and intermediate precision were calculated. In the first case, three different concentration levels were analyzed in triplicate (nine independent samples). On the other hand, the same three levels were evaluated in triplicate during three different weeks in order to compute intermediate precision,

i.e. a total of 27 independent samples. As can be appreciated, both results can be considered satisfactory as the CV% are all far below the 15% recommended by the European Medicines Agency in a document presented very recently [31].

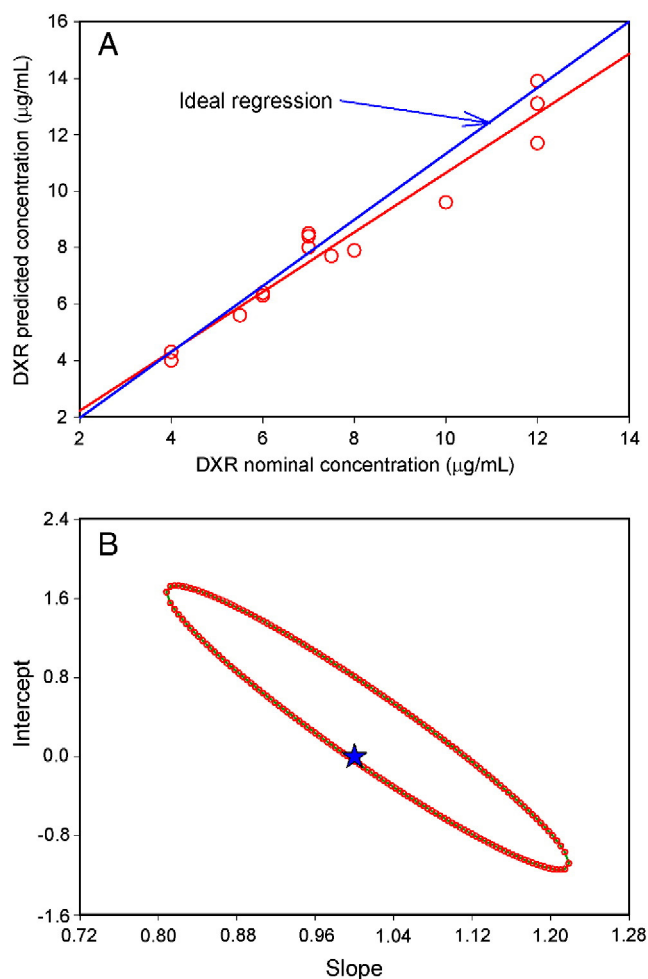


**Fig. 6.** (A) Nominal vs. predicted values plot and its corresponding least square fitting line. The ideal line corresponds to slope = 1 and intercept = 0. (B) Prediction region for the joint statistical test for the slope and the intercept of the linear regression between the nominal and predicted analyte concentrations of the global data set obtained with the extended MCR–ALS algorithm (95% of confidence). The star shows the theoretically expected values of the intercept (0) and the slope (1).

In addition, in order to compare the results obtained in each week and at every concentration level, an analysis of variance (ANOVA) was performed. Table 2 shows the obtained  $p$ -values, which are all higher than 0.05. In the three cases the null hypothesis was true, showing that no effect on the mean response is observed between weeks. Consequently, it can be concluded that the precision of the proposed method is acceptable.

#### 4.4.3. Predictions and accuracy

As it was commented in Section 2.5, validation samples 3 to 6 were spiked with different concentration levels of RFP. This was done in order to show the ability of the studied algorithm to achieve the second-order advantage. To predict DXR concentration in these validation samples, a  $\mathbf{D}$  augmented matrix was built by appending the second order data gathered for the validation mixtures together with those for the calibration samples. As it occurred with the calibration samples, when applying SVD to determine the correct number of compounds in the model, it was not possible to detect the right number of contributing components which explain the variance of the system. Therefore, based on the knowledge of the system under study three compounds were used. To build the initial estimation, the spectra of the acidic and basic

species of DXR, and the spectrum of RFP were obtained from the analysis of the purest spectra based on the SIMPLISMA methodology [27]. Although RFP has a  $pK_a = 7.9$  [32], its spectrum does not change with pH variations, and thus only one component was considered to model this interference.

The pseudounivariate calibration curve allowed us to predict the concentrations of the analyte in the validation samples (Table 3). The recovery values as well as the relative error of prediction were satisfactory (96 to 107%, and 3.1%, respectively). In order to compare the prediction results a paired  $t$ -test was carried out. The  $p$ -value for five degrees of freedom and  $\alpha = 0.05$  was 0.517, indicating that the null hypothesis was accepted. Consequently, it can be concluded that no significant differences exist between every pair, i.e. nominal vs. predicted values.

In addition, accuracy was assessed by comparing predicted vs. nominal analyte concentrations in the validation set (six samples), and in the samples used to perform the precision study (nine average values obtained from 27 samples). The comparison was made applying the joint statistical test for the slope and the intercept of the linear regression between the nominal and predicted analyte concentrations [33]. The multivariate model is accurate if the theoretical values of intercept and

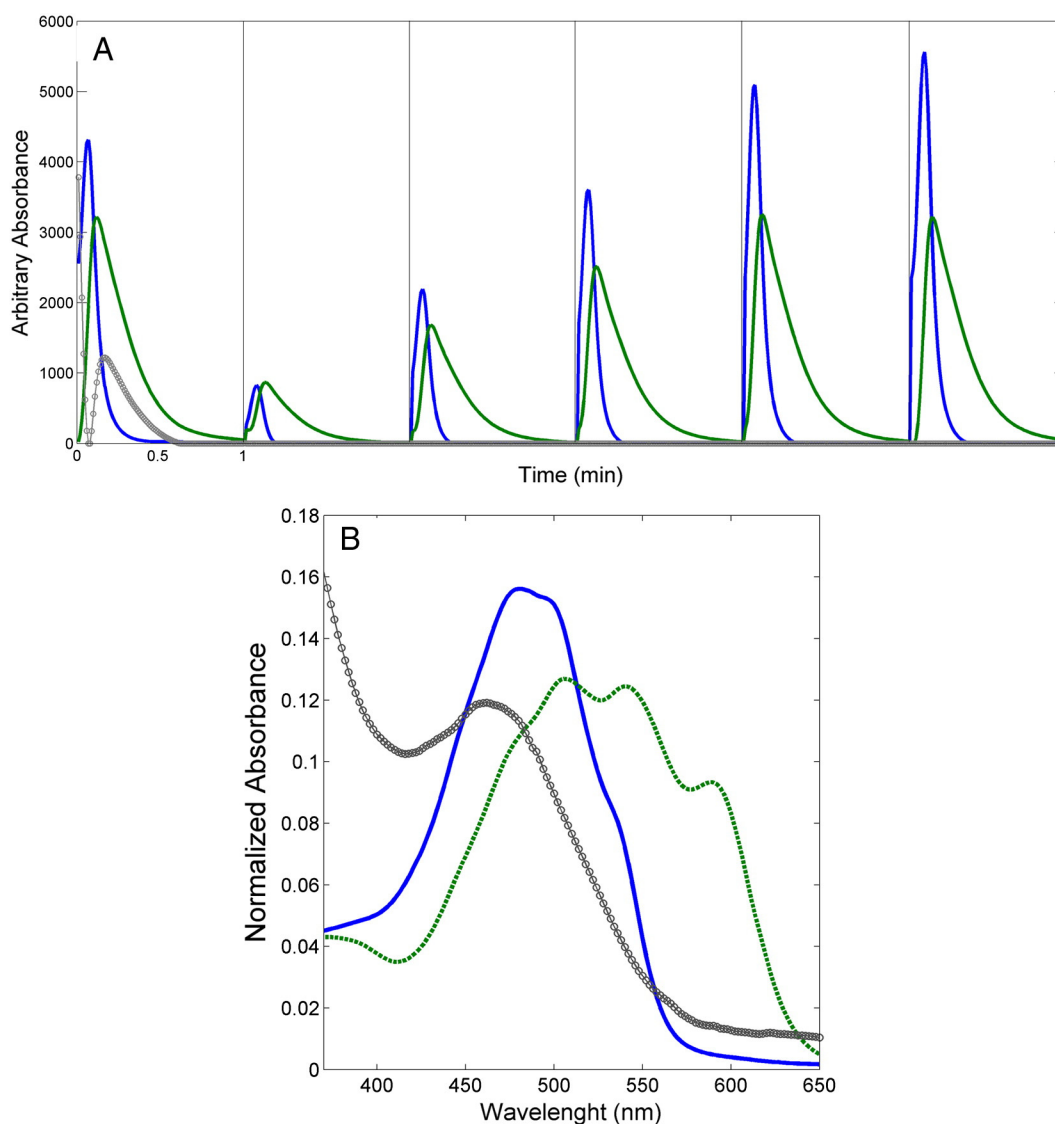


**Fig. 7.** (A) MCR-ALS FIA recovered profiles (solid blue line: DXR acidic form; dashed green line: DXR basic form; and circles gray line: RFP). (B) MCR-ALS spectral profiles for validation sample number 4 (solid blue line: DXR acidic form; dashed green line: DXR basic form; and circles gray line: RFP). (For interpretation of the references to color in this figure legend, the reader is referred to the web version of this article.)

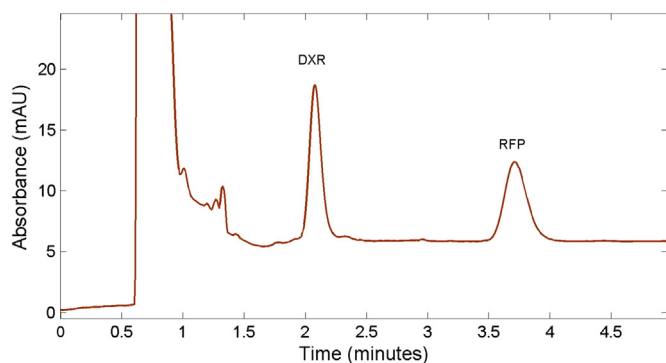


Fig. 8. Chromatogram registered at 254 nm for validation sample number 4 corresponding to a plasma sample spiked with DXR ( $7.5 \mu\text{g mL}^{-1}$ ) and RIF ( $14.3 \mu\text{g mL}^{-1}$ ).

slope (zero and unity, respectively) are included within the ellipse that describes the mutual confidence region. Fig. 6A shows the plot of nominal vs. predicted values and the corresponding least square fitting line. This figure also shows the ideal line which corresponds to slope = 1 and intercept = 0. Fig. 6B shows the prediction region of the global data set obtained with the extended MCR–ALS algorithm. As can be seen, the ellipse built with a confidence level of 95% contains the theoretically expected values for the intercept and the slope. This fact is indicative of the absence of both proportional and constant errors, in spite of the high spectral overlapping between the analyte species and the interference.

Finally, and in order to get further insight about the accuracy, two samples corresponding to the validation set were analyzed by HPLC following the procedure proposed by Alvarez et al. [34] adapted to present samples. The two studied samples were: (a) sample number 4 (plasma spiked with DXR at  $7.5 \mu\text{g mL}^{-1}$  and RIF at  $14.3 \mu\text{g mL}^{-1}$ ); and (b) sample number 5 (plasma spiked with DXR at  $6.0 \mu\text{g mL}^{-1}$  and RIF at  $12.5 \mu\text{g mL}^{-1}$ ). Fig. 8 shows the chromatogram registered at 254 nm corresponding to sample number 4. Results obtained by the comparative method are displayed in Table 3. A statistical *t*-test of comparison between average values obtained by both methods was performed allowing us to conclude that no significant difference exists ( $p = 0.09$  and  $0.07$ , respectively).

#### 4.4.4. Achieving physicochemical information

Fig. 7A shows the concentration profiles obtained for validation sample number 4 (see Table 3), and some of the calibration samples. Regarding the concentration gradient in this pH range, RFP ( $\text{pK}_{\text{RFP}} = 7.9$ ) has the same behavior as DXR, but its spectrum does not depend on pH. Because of this, the FIA profile of RFP presents only one compound whose shape is only determined by the sample dispersion.

The spectra of RFP and the two species of DXR provided by MCR–ALS are shown in Fig. 7B. In this figure it can be appreciated that the spectrum of RFP is highly overlapped with those of DXR, which could be a drawback in the mixture resolution. MCR–ALS results showed that the method was able to give some information about the interferent in the validation samples, i.e. RFP, by recovering both its pure spectra and flow-injection profile.

In order to quantitate the degree of spectral overlap ( $S_{12}$ ) between the spectra recovered by PKFIT ( $\mathbf{s}_1$ ) and MCR–ALS ( $\mathbf{s}_2$ ), the following expression was employed:

$$S_{12} = \frac{\|\mathbf{s}_1^T \mathbf{s}_2\|}{\|\mathbf{s}_1\| \|\mathbf{s}_2\|} \quad (5)$$

The value of  $S_{12}$  ranges from 0 to 1, corresponding to the extreme situation of no overlapping and complete overlapping, respectively. The application of the latter equation retrieved  $S_{12}$  values of 0.9997 and

0.9917 for the acidic and the basic species, respectively. These figures allow us to conclude that the modeling quality is highly satisfactory.

## 5. Conclusions

A pH-gradient FIA system with diode-array detection can be used to generate second-order data that can be conveniently managed to accurately determine DXR in human plasma. The second-order advantage allows for the quantitation of the analyte of interest in the presence of any number of uncalibrated compounds.

When managing this kind of data, a deep study of the acid–basic and concentration gradients in the FIA system properties should be performed in order to better exploit the potentiality of the generated data.

Extended MCR–ALS has proved to be a convenient algorithm to model this kind of data, which allows obtaining not only good analytical figures of merit, but also physicochemical interpretation of the systems under study.

In the light of these results, the present methodology can be recommended for the routine determination of DRX in plasma, with the possibility of being extended to other sort of samples owing the low LOQ obtained, i.e. application in environmental fields.

## Acknowledgments

The authors are grateful to Universidad Nacional del Litoral (Projects CAI + D 2011 N° 11-11 and 11-7), CONICET (Consejo Nacional de Investigaciones Científicas y Técnicas, Project PIP-2012 N° 455) and ANPcyT (Agencia Nacional de Promoción Científica y Tecnológica, Project PICT 2011-0005) for financial support. M.R.A. and A.V.S. thank CONICET for their fellowship.

## References

- [1] P.A. Speth, Q.G. van Hoesel, C. Haanen, Clinical pharmacokinetics of doxorubicin, *Clin. Pharmacokinet.* 15 (1988) 15–31.
- [2] R.S. Benjamin, C.E. Jr Riggs, N.R. Bachur, Pharmacokinetics and metabolism of adriamycin in man, *Clin. Pharmacol. Ther.* 14 (1973) 592–600.
- [3] S. Licata, A. Saponiero, A. Mordente, G. Minotti, Doxorubicin metabolism and toxicity in human myocardium: role of cytoplasmic deglycosidation and carbonyl reduction, *Chem. Res. Toxicol.* 13 (2000) 414–420.
- [4] V.T. DeVita, S.A. Rosenberg, S. Hellman, *Cancer, Principles and Practice of Oncology*, Lippincott, Williams & Wilkins, Philadelphia, 2001.
- [5] A. Andersen, D.J. Warren, L. Slordal, A sensitive and simple high-performance liquid chromatographic method for determination of doxorubicin and its metabolites in plasma, *Ther. Drug Monit.* 15 (1993) 455–461.
- [6] W.H. Gotlieb, I. Bruchim, G. Ben-Baruch, B. Davidson, A. Zeltser, A. Andersen, H. Olsen, Doxorubicin levels in the serum and ascites of patients with ovarian cancer, *EJSO* 33 (2007) 213–215.
- [7] C.L. Chen, K.K. Thoen, F.M. Uckun, High-performance liquid chromatographic methods for the determination of topoisomerase II inhibitors, *J. Chromatogr. B Biomed. Appl.* 764 (2001) 81–119.
- [8] P.M. Loadman, C.R. Calabrese, Separation methods for anthraquinone related anti-cancer drugs, *J. Chromatogr. B Biomed. Appl.* 764 (2001) 193–206.
- [9] O.T. Fahmy, M.A. Korany, H.M. Maher, High performance liquid chromatographic determination of some co-administered anticancer drugs in pharmaceutical preparations and in spiked human plasma, *J. Pharm. Biomed. Anal.* 34 (2004) 1099–1107.
- [10] R. DiFrancesco, J.J. Griggs, J. Donnelly, R. DiCenzo, Simultaneous analysis of cyclophosphamide, doxorubicin and doxorubicinol by liquid chromatography coupled to tandem mass spectrometry, *J. Chromatogr. B* 852 (2007) 545–553.
- [11] F. Lachâtre, P. Marquet, S. Ragot, J.M. Gaulier, P. Cardot, J.L. Dupuy, Simultaneous determination of four anthracyclines and three metabolites in human serum by liquid chromatography–electrospray mass spectrometry, *J. Chromatogr. B* 738 (2000) 281–291.
- [12] G. Zagotto, B. Gatto, S. Moro, C. Sissi, M. Palumbo, Anthracyclines: recent developments in their separation and quantitation, *J. Chromatogr. B Biomed. Appl.* 764 (2001) 161–171.
- [13] H. Lu, G. Yuan, Q. He, H. Chen, Rapid analysis of anthracycline antibiotics doxorubicin and daunorubicin by microchip capillary electrophoresis, *Microchem. J.* 92 (2009) 170–173.
- [14] J. Saurina, S. Hernández-Cassou, Quantitative determinations in conventional flow injection analysis based on different chemometric calibration strategies: a review, *Anal. Chim. Acta* 438 (2000) 335–352.
- [15] B. Karlberg, R. Torgrip, Increasing the scope and power of flow-injection analysis through chemometric approaches, *Anal. Chim. Acta* 500 (2003) 299–306.
- [16] M.J. Culzoni, H.C. Goicoechea, Determination of loratadine and pseudoephedrine sulfate in pharmaceuticals based on non-linear second order spectrophotometric

- data generated by a pH-gradient flow injection technique and artificial neural networks, *Anal. Bioanal. Chem.* 389 (2007) 2217–2225.
- [17] J. Saurina, S. Hernández-Cassou, A. Izquierdo-Ridorsa, R. Tauler, pH-Gradient spectrophotometric data files from flow-injection and continuous flow systems for two- and three-way data analysis, *Chemom. Intell. Lab. Syst.* 50 (2000) 263–271.
- [18] N.R. Marsili, A. Lista, B.S. Fernández Band, H.C. Goicoechea, A.C. Olivieri, A new method for the determination of benzoic and sorbic acids in commercial orange juices based on second-order spectrophotometric data generated by a pH gradient flow injection technique, *J. Agric. Food Chem.* 52 (2004) 2479–2484.
- [19] N.R. Marsili, A. Lista, B.S. Fernandez Band, H.C. Goicoechea, A.C. Olivieri, Evaluation of complex spectral-ph three-way arrays by modified bilinear least-squares: determination of four different dyes in interfering systems, *Analyst* 130 (2005) 1291–1298.
- [20] J. Saurina, Flow-injection analysis for multi-component determinations of drugs based on chemometric approaches, *TrAC Trends Anal. Chem.* 29 (2010) 1027–1037.
- [21] G.M. Escandar, N.M. Faber, H.C. Goicoechea, A. Muñoz de la Peña, A.C. Olivieri, R.J. Poppi, Second and third-order multivariate calibration: data, algorithms and applications, *TrAC Trends Anal. Chem.* 26 (2007) 752–765.
- [22] M.G. Trevisan, R.J. Poppi, Determination of doxorubicin in human plasma by excitation–emission matrix fluorescence and multi-way analysis, *Anal. Chim. Acta* 493 (2003) 69–81.
- [23] A.V. Schenone, M.J. Culzoni, A.D. Campiglia, H.C. Goicoechea, Total synchronous fluorescence spectroscopic data modeled with first- and second-order algorithms for the determination of doxorubicin in human plasma, *Anal. Bioanal. Chem.* (2013), doi:10.1007/s00216-013-7261-y (in press).
- [24] A. Avdeef, *Absorption and Drug Development: Solubility, Permeability, and Charge State*, Second ed. Wiley, New York, 2012.
- [25] MATLAB 7.10, The MathWorks Inc., Natick, Massachusetts, USA, 2010.
- [26] G.A. Ibañez, G.M. Escandar, A.C. Olivieri, Formation constants of copper(II)-salicylic acid complexes from multi-wavelength spectrophotometric pH titration data analyzed by alternating least-squares including Newton–Raphson and Gauss–Newton procedures, *Chem. Educ.* 12 (2007) 22–28.
- [27] W. Winding, J. Guilment, Interactive self-modeling mixture analysis, *Anal. Chem.* 63 (1991) 1425–1432.
- [28] J. Saurina, S. Hernández-Cassou, R. Tauler, A. Izquierdo-Ridorsa, Spectrophotometric determination of pK(a) values based on a pH gradient flow-injection system, *Anal. Chim. Acta* 408 (2000) 135–143.
- [29] S.A. Abraham, D.N. Waterhouse, L.D. Mayer, P.R. Cullis, T.D. Madden, M.B. Bally, The liposomal formulation of doxorubicin, *Method Enzymol.* 391 (2005) 71–97.
- [30] M.C. Bauza, G.A. Ibañez, R. Tauler, A.C. Olivieri, Sensitivity equation for quantitative analysis with multivariate curve resolution-alternating least-squares: theoretical and experimental approach, *Anal. Chem.* 84 (2012) 8697–8706.
- [31] [http://www.ema.europa.eu/docs/en\\_GB/document\\_library/Scientific\\_guideline/2011/08/WC500109686.pdf](http://www.ema.europa.eu/docs/en_GB/document_library/Scientific_guideline/2011/08/WC500109686.pdf) (European Medicines Agency, accessed May 2013).
- [32] M. Sosa, M.E. Széliga, A. Fernández, C. Bregni, Rifampicin and bioavailability in combination formulation, *ARS Pharm.* 46 (2005) 353–364.
- [33] J. Riu, F.X. Rius, Method comparison using regression with uncertainties in both axes, *Trends Anal. Chem.* 16 (1997) 211–216.
- [34] L. Alvarez-Cedron, M.L. Sayalero, J.M. Lanao, High-performance liquid chromatographic validated assay of doxorubicin in rat plasma and tissues, *J. Chromatogr. B* 721 (1999) 271–278.